Frequency response data-based peak filter design applied to MIMO large-scale high-precision scan stage

Masahiro Mae[a,*], Wataru Ohnishi[a], Hiroshi Fujimoto[a], Koichi Sakata[b], Atsushi Hara[b]

[a]*The University of Tokyo, 5-1-5, Kashiwanoha, Kashiwa, Chiba, 277-8561, Japan*
[b]*Nikon Corporation, 471, Nagaodaicho, Sakae, Yokohama, Kanagawa, 244-8533, Japan*

Abstract

A large-scale high-precision scan stage is important equipment in the industrial productions of micro-fabrication such as flat panel display (FPD) lithography systems. Designing controllers for multi-input multi-output (MIMO) systems is time-consuming and needs experience because of the interaction between each axis and many controller tuning parameters. The aim of this study is to develop a peak filter design method based on frequency response data to reduce repetitive disturbance. This data-based approach does not use the model and only uses the frequency response data of the controlled system and the disturbance spectrum calculated from the scanning error data (Contribution 1). The peak filter is designed by convex optimization and satisfies robust stability conditions for six-degree-of-freedom systems (Contribution 2). The control performance of the designed peak filter is experimentally demonstrated with an industrial MIMO large-scale high-precision scan stage in reducing the scanning error of the main stroke of the translation along the *x*-axis (Contribution 3).

Keywords: Concave-convex procedure; Data-based design; Frequency responses; Disturbance rejection; Peak filter; MIMO system

1. Introduction

Large-scale high-precision scan stages have an important role in industries such as manufacturing semiconductors and flat panel displays (FPD). To improve the throughput and the product quality, fast and precise positioning control is required, and these specifications become severe year by year because of the growing need for TVs, PCs, and smartphones [1].

The large-scale scan stage has several challenges in position control such as low resonance modes because of the low stiffness and many disturbances because of the wide scan range [2]. The large-scale scan stage is typically controlled with two-degree-of-freedom (DOF) control with a feedforward controller for reference tracking such as a perfect tracking control based on a multirate feedforward control [3, 4] and a feedback controller for disturbance rejection. In the scan region, the reference trajectory of the high-precision scan stage is with constant velocity without acceleration, and the feedback controller plays a major role in tracking control performance.

Classical scan stages move along (x, y, θ_z)-axes, and the interaction between each axis is ignored, and a single-input single-output (SISO) decentralized control is commonly employed. However, in these applications, the high-precision scan stages are supported by the magnetic force or air pressure and moving in 6-DOF with $(x, y, \theta_z, z, \theta_x, \theta_y)$-axes to reduce disturbances by the friction and the vibration from the ground and to improve tracking performance, and they become multi-input multi-output

(MIMO) systems [5, 6, 7, 8]. The controller design of the MIMO systems has several challenges such as stability analysis in a coupled system between each axis, modeling of MIMO systems, and enormous tuning parameters of the controllers. Especially, improving the tuning method of the controller parameters is important for the cost of time and effort of on-site control engineers.

Based on these challenges in designing the feedback controller, several data-based controller design approaches with an optimization method are proposed, such as genetic algorithm [9], Nelder-Mead method [10], particle swarm optimization [11], loop shaping method [12], bundle method [13, 14], sequential linearization method [15, 16, 17, 18] using concave-convex procedure [19].

Among these methods, the sequential linearization method using the concave-convex procedure has an advantage in monotonic convergence to a saddle point or a local optimum and suits for controller design. Other methods also need the parametric model of the controlled system. The precise modeling is difficult when the system is complicated such as MIMO systems.

In this study, the sequential linearization method using the concave-convex procedure is used with the frequency response data of the controlled system and disturbance spectrum to design the optimal feedback controller.

The disturbance spectrum during the scanning motion with constant velocity has a repetitive characteristic such as a motor cogging and has a large amplitude in a certain frequency.

The repetitive control approaches are presented to reject the periodic disturbances [20, 21, 22]. They reject the disturbance on not only main disturbance frequency but also harmonic ones.

The experimental setup in this study does not have a characteristic of harmonic disturbance frequencies, and the repetitive control approaches are not suitable for it.

Previous researches show that repetitive disturbance can be effectively rejected by a peak filter, which is the same as inverse notch filter in other literature, with the same resonance frequency, and it is applied in several industrial products such as hard disk drives [23]. However, in the application of the high-precision scan stage, the repetitive disturbance rejection by a peak filter has not been reported in the literature.

Since the peak filter has a large gain at a certain frequency, it may easily deteriorate the closed-loop stability due to the interaction. Moreover, the combination of the controller parameter can blow up in such a multi-axis system. Hence, the heuristic tuning approach [24] depends on experiences and efforts, and it is not the optimal solution. To address this problem, the frequency response data-based peak filter design method considering both the SISO robust stability condition and the MIMO stability condition is proposed in this study.

The optimal disturbance filter design method is also presented [25]. However, the peak filter is designed with nonlinear optimization procedure not with convex optimization. The convergence of the nonlinear optimization procedure is not monotonic and it could take a long time for the optimization. Therefore, the data-based peak filter design method with convex optimization suitable to industrial applications is proposed in this study.

The proposed peak filter design method has an advantage in convex optimization without parametric modeling. The control performance of the designed peak filter is experimentally demonstrated with an industrial MIMO large-scale high-precision scan stage in reducing the scanning error of the main stroke of the translation along the x-axis. This study consists of mainly these three following contributions:

Contribution 1. *The optimization problem of data-based peak filter design for the MIMO system is formulated.*

Contribution 2. *The data-based peak filter design method with convex optimization is presented.*

Contribution 3. *The designed peak filter is validated in the experiment with the industrial MIMO large-scale high-precision scan stage.*

2. Problem formulation

In this section, the control problem is formulated.

2.1. MIMO large-scale high-precision scan stage

The experimental setup is shown in Figure 1.

The experiment is conducted with the MIMO large-scale high-precision scan stage in the FPD lithography system which is 6-DOFs with six-inputs ($f_x, f_y, \tau_z, f_z, \tau_x, \tau_y$) and six-outputs ($x, y, \theta_z, z, \theta_x, \theta_y$).

The 6-DOFs stage is floating by the air bearing to cancel the gravity and frictions and actuated by voice coil motors and
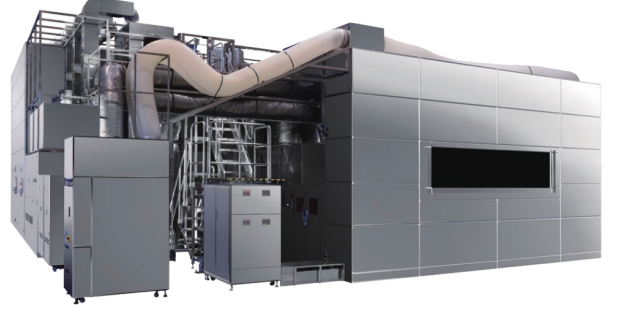

Figure 1: Experimental setup of FPD lithography system [26].

linear motors [6]. The positions and angles of the stage are measured by laser displacement sensors and linear encoders [24].

The frequency response of the experimental setup is shown in Figure 2.

The main stroke of the scan stage is the translation along the x-axis. The scan trajectory of translation along the x-axis is shown in Figure 3. The scan stage moves with the constant velocity through four scan regions at the same scanning procedure. The same controllers are used through four scan regions at the same scanning procedure.

2.2. Disturbance rejection with peak filter

Previous researches in high-precision positioning systems such as a hard disk drive show that a repetitive disturbance that has a large spectrum in a specific frequency is rejected by a peak filter that has the same resonance frequency [23] due to the internal model principle [27]. The transfer function of the peak filter is given by

$$F_{\text{Peak}}(j\omega, \rho, \eta) = \frac{s^2 + 2\rho\omega s + \omega^2}{s^2 + 2\eta\omega s + \omega^2} = \frac{F_n(j\omega, \rho)}{F_d(j\omega, \eta)}$$
$$(0 \le \eta < \rho \le 1), \tag{1}$$

where the resonance frequency is $\omega \in \mathbb{R}$, the damping coefficients are $\rho \in \mathbb{R}$ and $\eta \in \mathbb{R}$, and ρ must be larger than η in the peak filter. It is noted that it becomes a notch filter when ρ is smaller than η.

The scan stage moves with the constant velocity in the scan region and has several repetitive disturbances such as cogging. Therefore, the repetitive disturbance rejection approach with peak filter is applied to the MIMO large-scale high-precision scan stage. This approach has not been commonly used in the MIMO high-precision scan stage because the MIMO system high-gained by peak filter easily becomes unstable due to the interaction between each axis. In this study, the peak filter is designed with SISO robust stability condition and MIMO stability condition not to make the controlled system unstable.

2.3. Details of controlled system

The block diagram of the 6-DOF controlled system is shown in Figure 4. The 6-DOF controlled system P is given by frequency response data, as shown in Figure 2. The 6-DOF experimental setup is decoupled by the mechanical design and the thrust distribution.
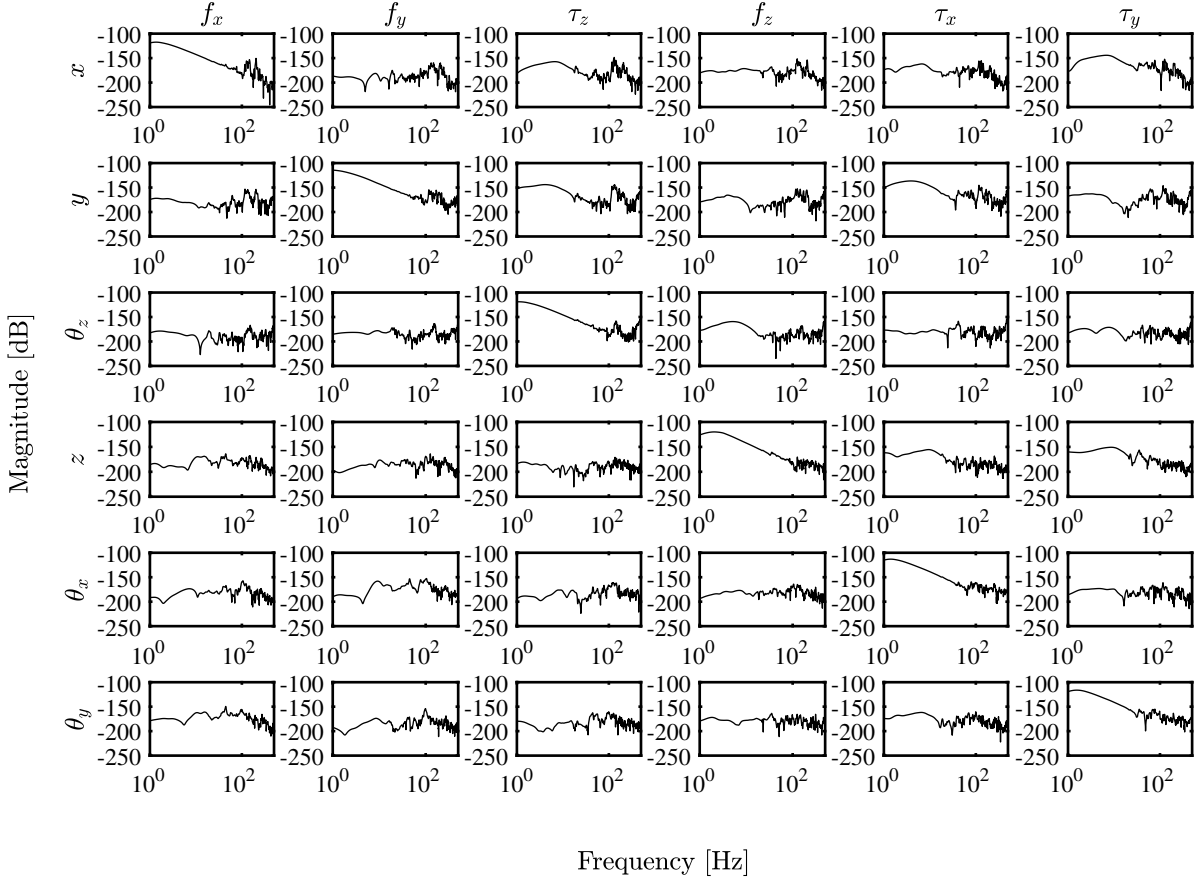
2

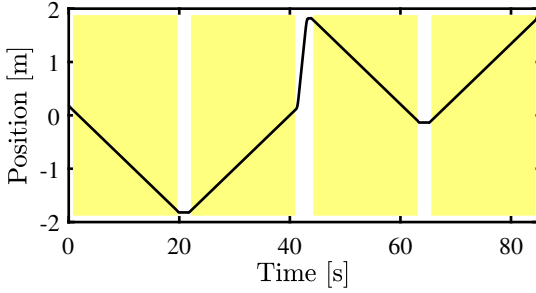Figure 2: Bode magnitude plot of 6-DOF experimental setup.

Figure 3: Scan trajectory of translation along the *x*-axis. The scan stage moves through four scan regions (▨) at the same scanning procedure. The scanning velocity of translation along the *x*-axis is set to 0.1 m/s.

The diagonal term in the frequency range less than about 10 Hz is modeled as a second-order rigid body system in each axis. The feedback controllers are conventionally designed with the model of the second-order rigid body systems in the only diagonal terms for the ease of the on-site final tuning process. In the proposed method, the peak filter can be designed with convex optimization using the frequency response data of the controlled system without the mathematical modeling of the large-scale MIMO high-precision scan stage.

The fixed diagonal feedback controller C that consists of

PID controllers, disturbance observers, phase lead filters, and notch filters is given beforehand. The diagonal peak filter F is designed with a proposed data-based design method.

The 6-DOF controlled system P, the fixed diagonal feedback controller C, and the diagonal peak filter F are defined as follows:

$$P(\mathrm{j}\omega_k) = P_{lm}(\mathrm{j}\omega_k), \tag{2}$$

$$C(\mathrm{j}\omega_k) = \begin{cases} C_l(\mathrm{j}\omega_k) & (l = m) \\ 0 & (l \neq m) \end{cases}, \tag{3}$$

$$F(\mathrm{j}\omega_k, \rho, \eta) = \begin{cases} \dfrac{F_{n_l}(\mathrm{j}\omega_k, \rho_l)}{F_{d_l}(\mathrm{j}\omega_k, \eta_l)} & (l = m) \\ 0 & (l \neq m) \end{cases}, \tag{4}$$

where $(l, m) \in \{x, y, \theta_z, z, \theta_x, \theta_y\}$ denotes the index of the 6-DOFs and the subscript k represents the frequency point of the frequency response data. The damping coefficients ρ and η of the peak filter are defined as follows:

$$\rho = \begin{bmatrix} \rho_x & \cdots & \rho_{\theta_y} \end{bmatrix}^\mathsf{T}, \tag{5}$$

$$\eta = \begin{bmatrix} \eta_x & \cdots & \eta_{\theta_y} \end{bmatrix}^\mathsf{T}. \tag{6}$$

2.4. Problem description and outline

In this study, the data-based peak filter design method is presented for the industrial MIMO large-scale high-precision
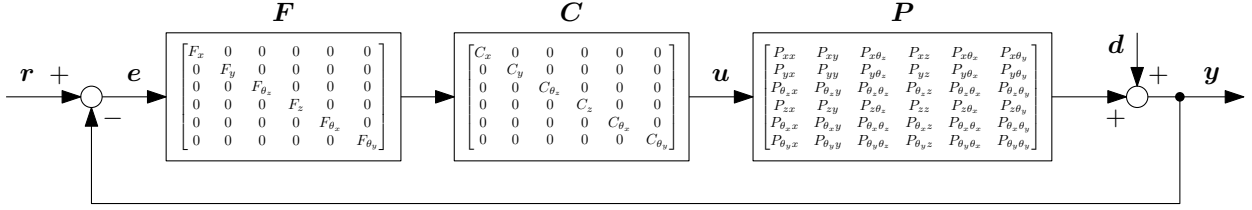
3

Figure 4: Block diagram of 6-DOF controlled system.

scan stage with respect to the following requirements:

Requirement 1. *The diagonal peak filter is designed with the fixed diagonal feedback controller and FRF data of the 6-DOF controlled system.*

Requirement 2. *The optimization problem is convex.*

Requirement 3. *The scanning error of the translation along the x-axis that is the main stroke of the scan stage should be reduced in the experiment.*

As is outlined in Section 1, pre-existing approaches fail to meet all requirements: the approaches with loop shaping method [12] and bundle method [13, 14] do not satisfy Requirement 1; the approaches with genetic algorithm [9], Nelder-Mead method [10], and particle swarm optimization [11] do not satisfy Requirement 2; the approach with sequential linearization method [15, 16, 17] using concave-convex procedure [19] does not satisfy Requirement 3. In summary, only the proposed approach satisfies the structured, diagonal, and convex optimized characteristics compared with other preexisting approaches.

In Section 3, the proposed data-based peak filter design method is presented that attains Requirement 1 through the weighting function of the sensitivity function with estimated disturbance spectrum, the SISO robust stability condition, and the MIMO stability condition, constituting Contribution 1. The convex optimization problem is formulated that attains Requirement 2 through sequential linearization method [15, 16, 17] using concave-convex procedure [19], constituting Contribution 2. In Section 4, the benefit of the approach that attains Requirement 3 is demonstrated through the experiment with the industrial MIMO large-scale high-precision scan stage, forming Contribution 3. In Section 5, conclusions are presented.

3. Data-based design method of peak filter with convex optimization

In this section, the data-based peak filter design method is formulated as a convex optimization problem. The proposed method is formulated to design the peak filters for the MIMO controlled system in each axis, independently.

3.1. Weighting function design for sensitivity function using disturbance spectrum

As shown in Figure 4, a sensitivity function S is a transfer function from the output disturbance d to the tracking error e.

The sensitive function S in Figure 4 is given by

$$S(j\omega_k) = (I + P(j\omega_k)C(j\omega_k)F(j\omega_k))^{-1}$$
$$= S_{lm}(j\omega_k), \tag{7}$$

and the output disturbance d and the tracking error e are also given by

$$d(j\omega_k) = \begin{bmatrix} d_x(j\omega_k) & \cdots & d_{\theta_y}(j\omega_k) \end{bmatrix}^\mathsf{T}, \tag{8}$$

$$e(j\omega_k) = \begin{bmatrix} e_x(j\omega_k) & \cdots & e_{\theta_y}(j\omega_k) \end{bmatrix}^\mathsf{T}. \tag{9}$$

The output disturbance d does not deteriorate the tracking error e within the frequency in which the gain of the sensitivity function S is low. Therefore, the weighting function of the sensitivity function is designed from the disturbance spectrum of the scanning motion.

The output disturbance spectrum estimated from the tracking error of the scanning motion is given by

$$d(j\omega_k) = S^{-1}(j\omega_k)e(j\omega_k). \tag{10}$$

The weighting function of the sensitivity function using the output disturbance spectrum [28] is given by

$$W_S(j\omega_k) = \begin{bmatrix} W_{S_x}(j\omega_k) & \cdots & W_{S_{\theta_y}}(j\omega_k) \end{bmatrix}^\mathsf{T}, \tag{11}$$

where

$$|W_{S_l}(j\omega_k)| = \alpha_l|d_l(j\omega_k)|, \tag{12}$$

and α_l is a scaling parameter.

The feedback controller is designed to satisfy the condition of the sensitivity function as follows:

$$|S_{ll}(j\omega_k)W_{S_l}(j\omega_k)| \le 1. \tag{13}$$

As shown in Figure 5, when the scaling parameter α_l becomes large, $1/W_{S_l}$ goes down. Therefore, the effective disturbance rejection is achieved when the condition (13) is satisfied in a larger scaling parameter α_l.

3.2. SISO robust stability condition with circle condition for gain margin and phase margin

In this study, the stability condition of the controlled system is analyzed by the Nyquist stability theorem. The SISO robust stability condition is considered with circle condition calculated from the gain margin g_m and the phase margin Φ_m [29].
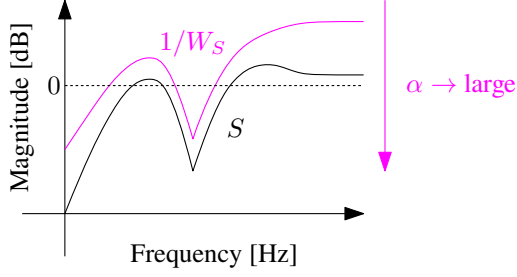
4

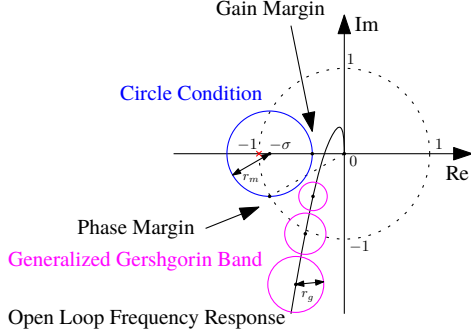Figure 5: Sensitivity function with disturbance spectrum weighting function.

Figure 6: Circle condition of gain margin, phase margin and generalized Gershgorin bands.

The center $(-\sigma, 0\mathrm{j})$ and radius r_m of a circle condition on the Nyquist diagram is given by

$$\sigma = \frac{g_m^2 - 1}{2g_m(g_m \cos \Phi_m - 1)}, \tag{14}$$

$$r_m = \frac{(g_m - 1)^2 + 2g_m(1 - \cos \Phi_m)}{2g_m(g_m \cos \Phi_m - 1)}. \tag{15}$$

As shown in Figure 6, when the controller is stable and the open-loop frequency response does not cross the circle condition on the Nyquist diagram, the controller satisfies the SISO robust stability condition for the gain margin g_m and the phase margin Φ_m.

3.3. MIMO stability condition with generalized Gershgorin bands

The MIMO controlled system may become unstable due to the interaction between each axis even if the SISO controlled system in each axis is stable. The MIMO stability condition is considered in the Direct Nyquist Array (DNA) method with generalized Gershgorin bands [30, 31, 32].

In the DNA method, the interaction index $\lambda(\mathrm{j}\omega_k | \boldsymbol{P})$ of the controlled system $\boldsymbol{P}$ is defined as a maximum eigenvalue of $\boldsymbol{M}(\mathrm{j}\omega_k | \boldsymbol{P})$, where the matrix $\boldsymbol{M}(\mathrm{j}\omega_k | \boldsymbol{P})$ is given by

$$\boldsymbol{M}(\mathrm{j}\omega_k | \boldsymbol{P}) = \begin{cases} 0 & (l = m) \\ \left| \frac{P_{lm}(\mathrm{j}\omega_k)}{P_{mm}(\mathrm{j}\omega_k)} \right| & (l \neq m) \end{cases}. \tag{16}$$

The radius r_{g_l} of the generalized Gershgorin bands is given by

$$r_{g_l}(\mathrm{j}\omega_k) = \lambda(\mathrm{j}\omega_k) \left| \frac{P_{ll}(\mathrm{j}\omega_k)C_l(\mathrm{j}\omega_k)F_{n_l}(\mathrm{j}\omega_k, \rho)}{F_{d_l}(\mathrm{j}\omega_k, \eta)} \right|. \tag{17}$$

The open-loop frequency response of each axis may move within the radius at each frequency point on the Nyquist diagram when MIMO systems have the interaction between each axis. As shown in Figure 6, when the controller is stable and the generalized Gershgorin bands do not include the point of $(-1, 0\mathrm{j})$ on the Nyquist diagram, the controlled system satisfies a MIMO stability condition with the interaction between each axis.

3.4. Optimization problem formulation

The optimization problem to design a peak filter with a disturbance spectrum, a SISO robust stability condition, and a MIMO stability condition is formulated from (18) to (22).

$$\underset{\rho_l, \eta_l}{\text{maximize}} \quad \alpha_l \tag{18}$$

subject to
$$\forall k$$

$$|W_{S_l}(\mathrm{j}\omega_k)| - \left| \frac{P_{ll}(\mathrm{j}\omega_k)C_l(\mathrm{j}\omega_k)F_{n_l}(\mathrm{j}\omega_k, \rho_l)}{F_{d_l}(\mathrm{j}\omega_k, \eta_l)} + 1 \right| \leq 0 \tag{19}$$

$$r_m - \left| \frac{P_{ll}(\mathrm{j}\omega_k)C_l(\mathrm{j}\omega_k)F_{n_l}(\mathrm{j}\omega_k, \rho_l)}{F_{d_l}(\mathrm{j}\omega_k, \eta_l)} + \sigma \right| \leq 0 \tag{20}$$

$$r_{g_l}(\mathrm{j}\omega_k) - \left| \frac{P_{ll}(\mathrm{j}\omega_k)C_l(\mathrm{j}\omega_k)F_{n_l}(\mathrm{j}\omega_k, \rho_l)}{F_{d_l}(\mathrm{j}\omega_k, \eta_l)} + 1 \right| \leq 0 \tag{21}$$

$$0 \leq \beta\eta_l \leq \rho_l \leq 1 \quad (\beta > 1) \tag{22}$$

3.5. Concave-convex procedure

There are two challenges in solving this optimization problem with convex optimization. First, the peak filter has tuning parameters not only in the numerator but also in the denominator. Second, the constraints of the formulated optimization problem are non-convex functions because of the difference of the convex functions. To solve these challenges, a sequential linearization method using concave-convex procedure [19] with tuning parameters in both the numerator and the denominator [33] is applied to this optimization problem.

First, the denominator $|F_d(\mathrm{j}\omega_k, \eta)|$ is multiplied on both sides of the constraints, as shown in (23), (24), and (25). Second, a first-order approximation of the difference term of the constraints is calculated, as shown in (26), (27), and (28). From these two procedures, the constraints of the optimization problem become convex in the current operating point. It is noted that $\rho_{l_{i-1}}$ and $\eta_{l_{i-1}}$ are the values of the optimization result in the previous iteration, and this optimization problem can be solved as a convex optimization problem with iterative calculations. In this study, a dichotomy method is used for an iterative calculation algorithm.

4. Experimental validation

In this section, experimental validation is conducted. The aim of this study is to develop a peak filter design method based on frequency response data. The control performance of the designed peak filter is experimentally demonstrated with an industrial MIMO large-scale high-precision scan stage in reducing the scanning error of the main stroke of the translation along the x-axis.

$$|W_{S_l}(\mathrm{j}\omega_k)F_{d_l}(\mathrm{j}\omega_k,\eta_l)| - |P_{ll}(\mathrm{j}\omega_k)C_l(\mathrm{j}\omega_k)F_{n_l}(\mathrm{j}\omega_k,\rho_l) + F_{d_l}(\mathrm{j}\omega_k,\eta_l)| \leq 0 \tag{23}$$

$$r_m|F_{d_l}(\mathrm{j}\omega_k,\eta_l)| - |P_{ll}(\mathrm{j}\omega_k)C_l(\mathrm{j}\omega_k)F_{n_l}(\mathrm{j}\omega_k,\rho_l) + \sigma F_{d_l}(\mathrm{j}\omega_k,\eta_l)| \leq 0 \tag{24}$$

$$r_{g_l}(\mathrm{j}\omega_k)|F_{d_l}(\mathrm{j}\omega_k,\eta_l)| - |P_{ll}(\mathrm{j}\omega_k)C_l(\mathrm{j}\omega_k)F_{n_l}(\mathrm{j}\omega_k,\rho_l) + F_{d_l}(\mathrm{j}\omega_k,\eta_l)| \leq 0 \tag{25}$$

$$|W_{S_l}(\mathrm{j}\omega_k)F_{d_l}(\mathrm{j}\omega_k,\eta_l)| - \mathrm{Re}\left(\frac{(P_{ll}(\mathrm{j}\omega_k)C_l(\mathrm{j}\omega_k)F_{n_l}(\mathrm{j}\omega_k,\rho_{l_{i-1}}) + F_{d_l}(\mathrm{j}\omega_k,\eta_{l_{i-1}}))^*}{|P_{ll}(\mathrm{j}\omega_k)C_l(\mathrm{j}\omega_k)F_{n_l}(\mathrm{j}\omega_k,\rho_{l_{i-1}}) + F_{d_l}(\mathrm{j}\omega_k,\eta_{l_{i-1}})|}(P_{ll}(\mathrm{j}\omega_k)C_l(\mathrm{j}\omega_k)F_{n_l}(\mathrm{j}\omega_k,\rho_{l_i}) + F_{d_l}(\mathrm{j}\omega_k,\eta_{l_i}))\right) \leq 0 \tag{26}$$

$$r_m|F_{d_l}(\mathrm{j}\omega_k,\eta_{l_i})| - \mathrm{Re}\left(\frac{(P_{ll}(\mathrm{j}\omega_k)C_l(\mathrm{j}\omega_k)F_{n_l}(\mathrm{j}\omega_k,\rho_{l_{i-1}}) + \sigma F_{d_l}(\mathrm{j}\omega_k,\eta_{l_{i-1}}))^*}{|P_{ll}(\mathrm{j}\omega_k)C_l(\mathrm{j}\omega_k)F_{n_l}(\mathrm{j}\omega_k,\rho_{l_{i-1}}) + \sigma F_{d_l}(\mathrm{j}\omega_k,\eta_{l_{i-1}})|}(P_{ll}(\mathrm{j}\omega_k)C_l(\mathrm{j}\omega_k)F_{n_l}(\mathrm{j}\omega_k,\rho_{l_i}) + \sigma F_{d_l}(\mathrm{j}\omega_k,\eta_{l_i}))\right) \leq 0 \tag{27}$$

$$r_{g_l}(\mathrm{j}\omega_k)|F_{d_l}(\mathrm{j}\omega_k,\eta_l)| - \mathrm{Re}\left(\frac{(P_{ll}(\mathrm{j}\omega_k)C_l(\mathrm{j}\omega_k)F_{n_l}(\mathrm{j}\omega_k,\rho_{l_{i-1}}) + F_{d_l}(\mathrm{j}\omega_k,\eta_{l_{i-1}}))^*}{|P_{ll}(\mathrm{j}\omega_k)C_l(\mathrm{j}\omega_k)F_{n_l}(\mathrm{j}\omega_k,\rho_{l_{i-1}}) + F_{d_l}(\mathrm{j}\omega_k,\eta_{l_{i-1}})|}(P_{ll}(\mathrm{j}\omega_k)C_l(\mathrm{j}\omega_k)F_{n_l}(\mathrm{j}\omega_k,\rho_{l_i}) + F_{d_l}(\mathrm{j}\omega_k,\eta_{l_i}))\right) \leq 0 \tag{28}$$

4.1. Experimental setup

The experimental setup is shown in Figure 1. In this setup, the MIMO large-scale high-precision scan stage moves with the constant velocity through four scan regions at the same scanning procedure as shown in Figure 3. In this study, the scanning velocity of translation along the x-axis is set to 0.1 m/s. The frequency response of the 6-DOF experimental setup, as shown in Figure 2, and the scanning error data are collected by pre-experiment and used for the peak filter design.

4.2. Data-based peak filter design conditions

The peak filter is designed by the convex optimization with the frequency response of the 6-DOF experimental setup and the scanning error data. The number of frequency response data points is set to 1000, and they are arranged at logarithmically even intervals in the range from 1 Hz to 500 Hz. The error spectrum and disturbance spectrum are averaged in four scan regions to consider four scan regions with the same designed peak filter.

The flowchart of the proposed peak filter design method is shown in Figure 7. In this study, only one peak filter is designed in translation along the x-axis that is the main stroke of the scan stage, and the peak filters in other axes are set to 1. The frequency response data of C_x that is fixed feedback controller along the x-axis consisting of PID controller, disturbance observer, phase lead filter, and notch filter is shown in Figure 8.

The resonance frequency of the peak filter in translation along the x-axis is set to a constant frequency $\omega_x = 41.1$ rad/s ($f_x = \omega_x/2\pi = 6.54$ Hz) in which the power spectra of the scanning error is the maximum. From the difference of the disturbance spectrum at the peak and peripheral frequency, the gain of the peak filter should be larger than 6 dB (≈ 2). Therefore, the minimum gain of the peak filter is set to $\beta = 6$ dB (≈ 2) in the parameter constraints (22). The initial value of each parameter is set to $\rho_x^{\mathrm{ini}} = 1 \times 10^{-2}$ and $\eta_x^{\mathrm{ini}} = 1 \times 10^{-3}$, respectively. It is noted that the initial condition is set to be a feasible solution.

The gain margin and the phase margin in the SISO robust stability condition are set to $g_m = 4$ dB and $\Phi_m = 20$ deg, respectively. This condition is satisfied in the controlled system without a peak filter.

In the MIMO stability condition, the generalized Gershgorin bands are considered only in the frequency range $f_c/2 \leq f < 2f_c$, when f_c is the gain cross over frequency of the open-loop transfer function without using the peak filter. The MIMO stability condition with the generalized Gershgorin bands is a sufficient condition, and the controlled system should not be designed too conservative. Therefore, only this frequency range in which the stability condition is most affected is considered in the MIMO stability condition. In other frequencies, the interference index is set to $\lambda(\mathrm{j}\omega_k) = 0$.

The dichotomy method is used to solve the convex optimization problem with a sequential linearization method using concave-convex procedure. The output disturbance spectrum along the x-axis used for the weighting function of the sensitivity function with the scaling parameter α_x is shown in Figure 9. The main reason of the disturbance in the frequency range of from 5 Hz to 10 Hz is the vibrations from a coarse stage and a ground transmitted through the gravity canceller [24].

The objective function α_x is searched in the range of $\alpha_x^{\mathrm{min}} = 1 \times 10^5$ and $\alpha_x^{\mathrm{max}} = 1 \times 10^7$. The sensitivity function without peak filter and the weighting functions with the initial conditions are shown in Figure 10. The Nyquist diagram without a peak filter is shown in Figure 11. The Nyquist diagram with the initial peak filter is shown in Figure 12.

In the proposed peak filter design method, parametric model of the controlled system and the given controller are not needed, and the frequency response data of them are enough for designing the peak filter.

The iterative optimization by the dichotomy method is repeated until $\frac{\alpha_x^{\mathrm{ng}}}{\alpha_x^{\mathrm{ok}}} \leq 1.01$, where α_x^{ok} and α_x^{ng} are defined as the values of α_x in the feasible and infeasible solutions, respectively. The optimization calculation searches the feasible set of the parameter with larger ρ in the current operating point to design a peak filter with a wider resonance peak. The optimization problem is calculated by YALMIP [34] and Mosek [35].

4.3. Optimization results

By the optimization calculation, the values of the objective function and the optimal peak filter are given by $\alpha_x^{\mathrm{opt}} = 1482520$, $\rho_x^{\mathrm{opt}} = 0.02325$, and $\eta_x^{\mathrm{opt}} = 0.011653$, respectively.
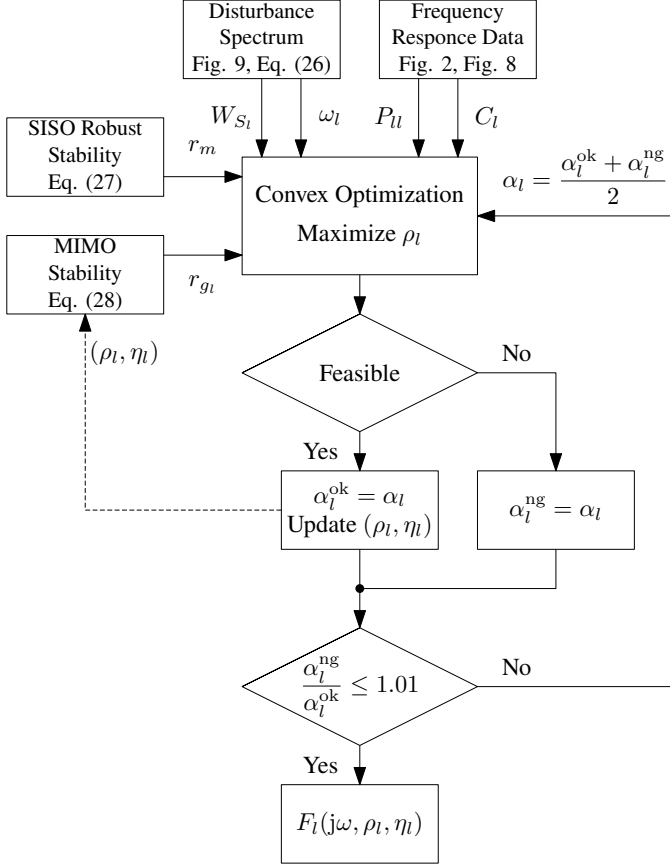
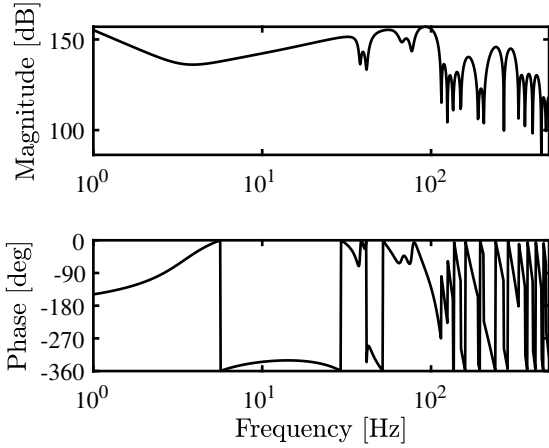Figure 7: Flowchart of proposed peak filter design method.

Figure 8: Frequency response data of C_x that is fixed feedback controller along x-axis consisting of PID controller, disturbance observer, phase lead filter, and notch filter.

The sensitivity function and the weighting function with the initial and the optimal peak filter are shown in Figure 13. It is confirmed that the controller gain at the frequency of the maximum error spectrum becomes high due to using the peak filter, and the gain of the sensitivity function becomes low.

The Nyquist diagram with the optimal peak filter is shown in Figure 14. It is confirmed that the designed controller sat-
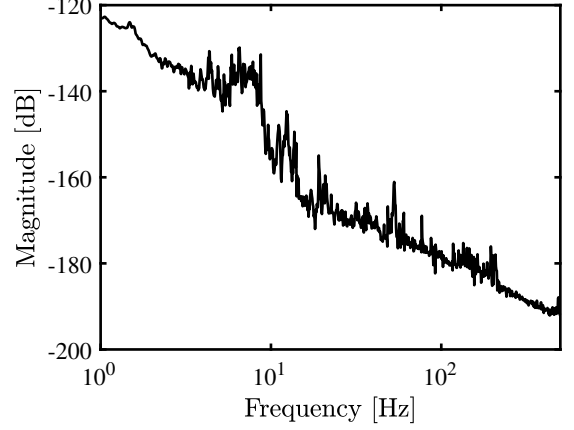
Figure 9: Output disturbance spectrum along x-axis used for weighting function of sensitivity function with scaling parameter α_x.

isfies both the SISO robust stability condition and the MIMO stability condition.

4.4. Simulation evaluation

The simulation evaluation is conducted before the experiment.

The error with the peak filter $e^{\mathrm{w}}(\mathrm{j}\omega_k)$ is calculated from the sensitivity function with and without the peak filter, $S^{\mathrm{w}}(\mathrm{j}\omega_k)$ and $S(\mathrm{j}\omega_k)$, and the error without the peak filter $e(\mathrm{j}\omega_k)$ as follows:

$$
\begin{aligned}
e^{\mathrm{w}}(\mathrm{j}\omega_k) =& S^{\mathrm{w}}(\mathrm{j}\omega_k)S^{-1}(\mathrm{j}\omega_k)e(\mathrm{j}\omega_k) \\
=& (I + P(\mathrm{j}\omega_k)C(\mathrm{j}\omega_k)F(\mathrm{j}\omega_k,\rho,\eta))^{-1} \\
& (I + P(\mathrm{j}\omega_k)C(\mathrm{j}\omega_k))e(\mathrm{j}\omega_k).
\end{aligned} \tag{29}
$$

The time series of the simulated scanning errors of translation along the x-axis in four scan regions are calculated by inverse Fourier transform as shown in Figure 15. The unit "[count]" means the resolution of the measurement sensor in the setup. From the simulation results, the optimized peak filter outperforms the without and with the initial peak filters.

4.5. Experimental results

The experimental validation is conducted without and with the peak filter. In the conventional methods, the peak filter cannot be designed with convex optimization using the frequency response data of the controlled system, not using the model of the controlled system. Therefore, the feedback controller without peak filter is used as the conventional method in the experimental validation.

The time series of the scanning errors of translation along the x-axis in four scan regions are shown in Figure 16. The amplitude spectra of the scanning errors of translation along the x-axis in four scan regions are also shown in Figure 17.

The scanning error is effectively reduced in scan region 1 and 4, as shown in Figure 16(a) and Figure 16(d). The disturbance around 6.54 Hz is effectively rejected by the peak filter and the scanning error is also reduced, as shown in Figure 17(a)
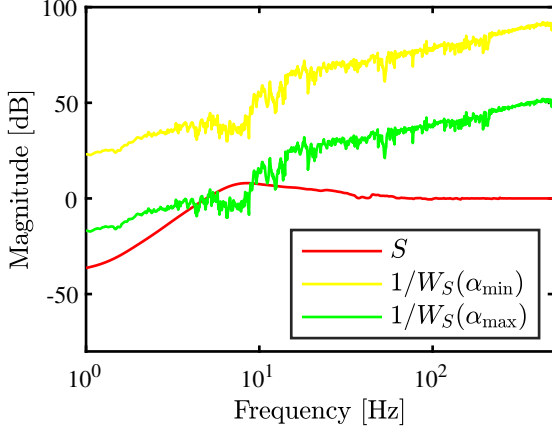
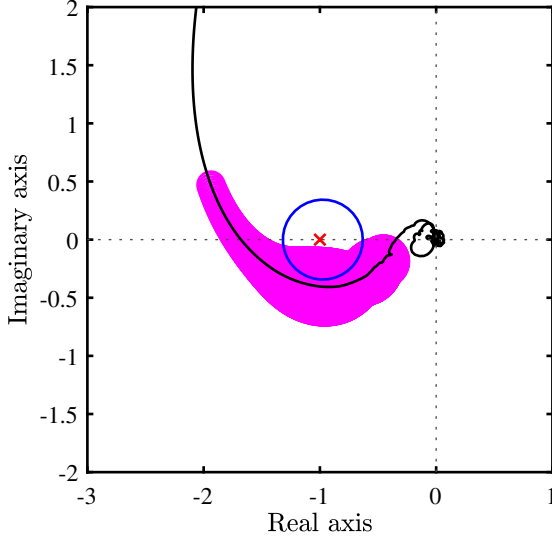Figure 10: Sensitivity function and weighting function without peak filter of translation along the x-axis.

Figure 11: Nyquist diagram without peak filter of translation along the x-axis.

Figure 12: Nyquist diagram with initial condition of translation along the x-axis.

and Figure 17(d). From this result, the effectiveness of the peak filter in disturbance rejection is validated.

On the other hand, the scanning error is not dramatically changed in scan regions 2 and 3, as shown in Figure 16(b) and Figure 16(c). This is because the frequency of the peak amplitude of the scanning error spectra in scan region 2 and 3 is around 7.5 Hz, and the disturbance in this frequency range can not be effectively rejected by the designed peak filter with the resonance frequency $f_x = 6.54$ Hz.

The Root Mean Square (RMS) errors of a total of four scan regions in 6-DOFs $(x, y, \theta_z, z, \theta_x, \theta_y)$ are shown in Figure 18. Figure 18(a) shows that the RMS error in translation along the x-axis that is the main stroke of the scan stage is reduced. It means that the average scan quality is improved and the effectiveness of the designed peak filter is validated. It is also noteworthy that the RMS errors in (y, θ_z, z)-axes are also improved. It is because that the interaction of the disturbance from the x-axis is reduced by the peak filter. On the other hand, the RMS errors in (θ_x, θ_y)-axes are increased. It is because that the inter-

action of the control input from the x-axis is increased by the feedback controller high-gained by the peak filter. From these discussions, the peak filter has the advantage to reject the disturbance and to reduce the scanning error in the MIMO large-scale high-precision scan stage.

In this study, the feedback controller is designed diagonally as a setup restriction and human friendliness for the manual tuning in the industrial final introduction process. In this case, the coupling effect cannot be completely suppressed by the feedback controller because of not enough degree of freedom. Therefore, the disturbance rejection performance of the main scan x-axis is mainly concerned, and only the MIMO stability condition is comprised in the peak filter design. Several decoupling control techniques are also proposed from both sides of the linear and the nonlinear control approach [36, 37]. The physical and mathematical analysis of coupling effect by the designed peak filter and decoupling controller design is ongoing study.

Further improvement is possible with additional peak filters in the x-axis or other axes. The proposed peak filter design method can be applied to other axes with the MIMO stability condition. However, MIMO robust performance improvement is not guaranteed. Therefore, the decoupling controller also should be designed at the same time with designed peak filters in multi-axes. It also should be concerned that the additional stability margin is needed to design the additional peak filters because of the phase lag after the resonance frequency. To deal with this problem, the phase compensator should be designed simultaneously as the peak filter, or all controllers should be optimized at once.

5. Conclusion

The frequency response data-based peak filter design in this study enables reducing tracking errors in the scanning motion. The main underlying idea of this study is the combination of
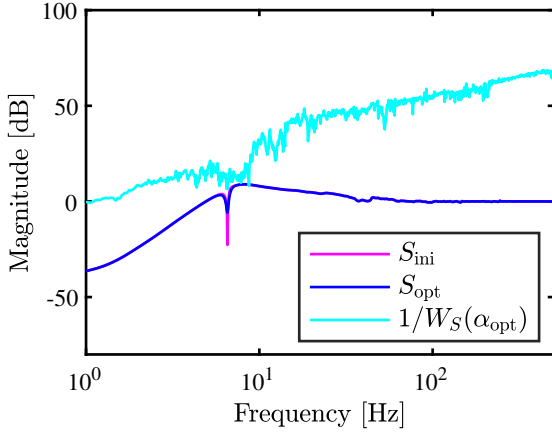
Figure 13: Sensitivity function and weighting function with optimal condition of translation along the x-axis.
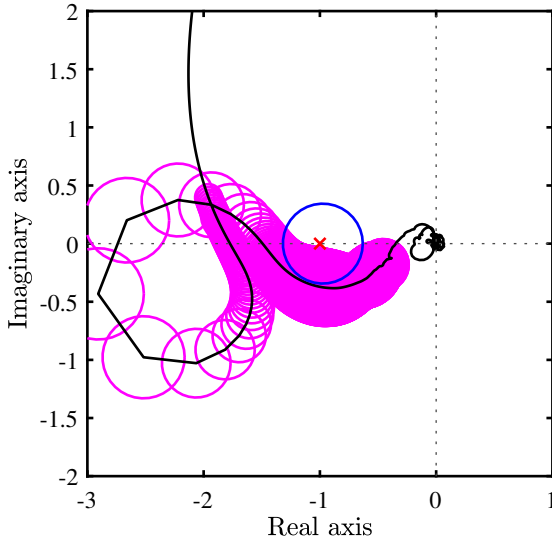

Figure 14: Nyquist diagram with optimal condition of translation along the x-axis.

the frequency response data-based design approach with convex optimization and the robust design method of the MIMO controlled systems.

The effectiveness of the designed peak filter is demonstrated in the experiment with the industrial MIMO large-scale high-precision scan stage. The disturbance spectrum of the maximum error frequency is effectively rejected by the designed peak filter, and as a result, it is confirmed that the scanning error spectrum of that frequency is reduced.

Ongoing research focuses on designing additional peak filters with phase compensators and total optimization that includes not only peak filters but also other controllers.
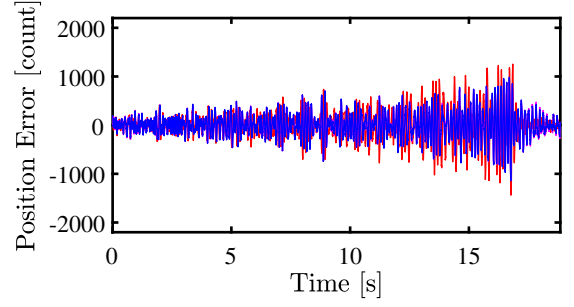
(a) Scan region 1.
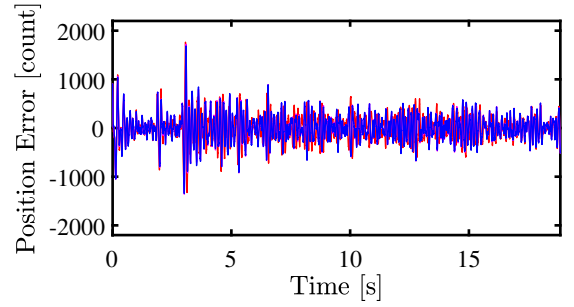
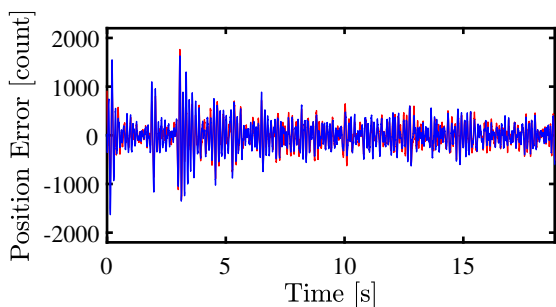(b) Scan region 2.
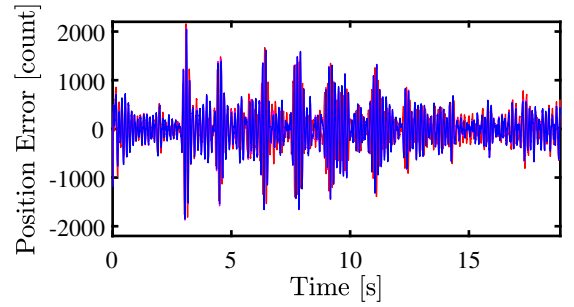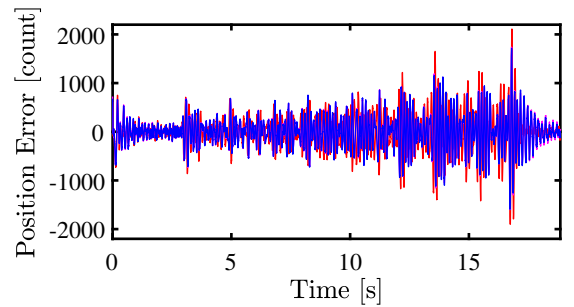
(c) Scan region 3.
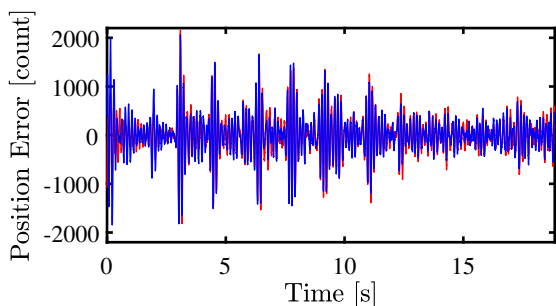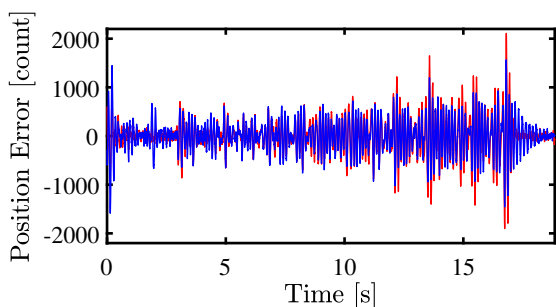

(d) Scan region 4.

Figure 15: Simulated position error of translation along the x-axis in four scan regions. No peak filter is used in w/o (——), one peak filter of translation along the x-axis with initial condition is used in (——), and one peak filter of translation along the x-axis with optimized condition is used in w/ (——). Errors in one peak filter of translation along the x-axis with initial and optimized conditions are overlapped but a little improved in the optimized condition.
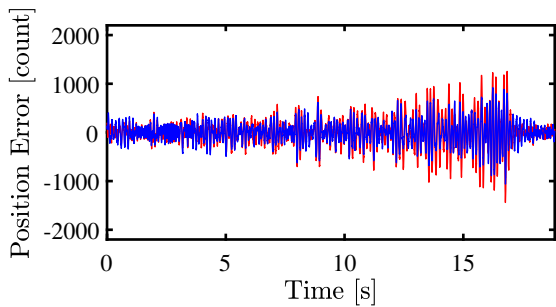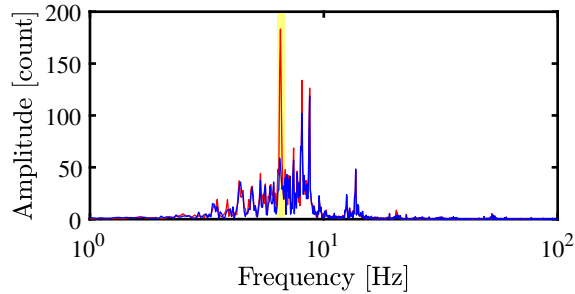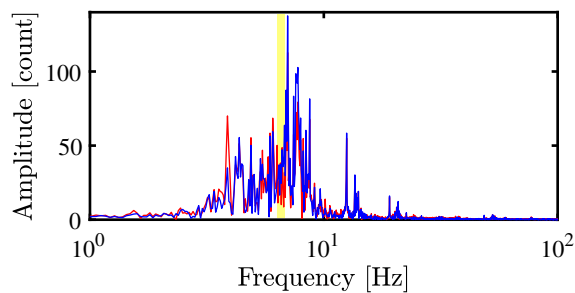
9

(a) Scan region 1.

(b) Scan region 2.

(c) Scan region 3.
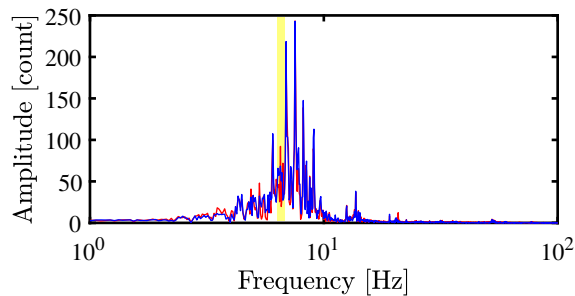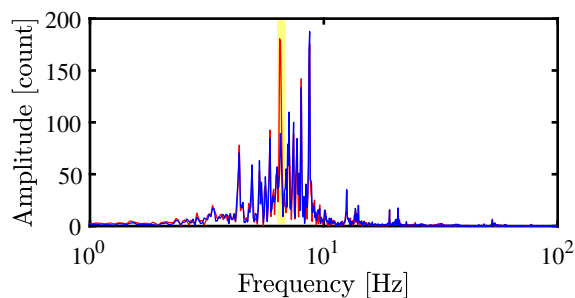
(d) Scan region 4.

Figure 16: Position error of translation along the *x*-axis in four scan regions. No peak filter is used in w/o (———) and one peak filter of translation along the *x*-axis is used in w/ (———).

Figure 17: Amplitude spectrum of position error of translation along the *x*-axis in four scan regions. No peak filter is used in w/o (———) and one peak filter of translation along the *x*-axis with optimized condition is used in w/ (———). The frequency range around the resonance frequency of the designed peak filter (6.54 Hz) is highlighted (■).
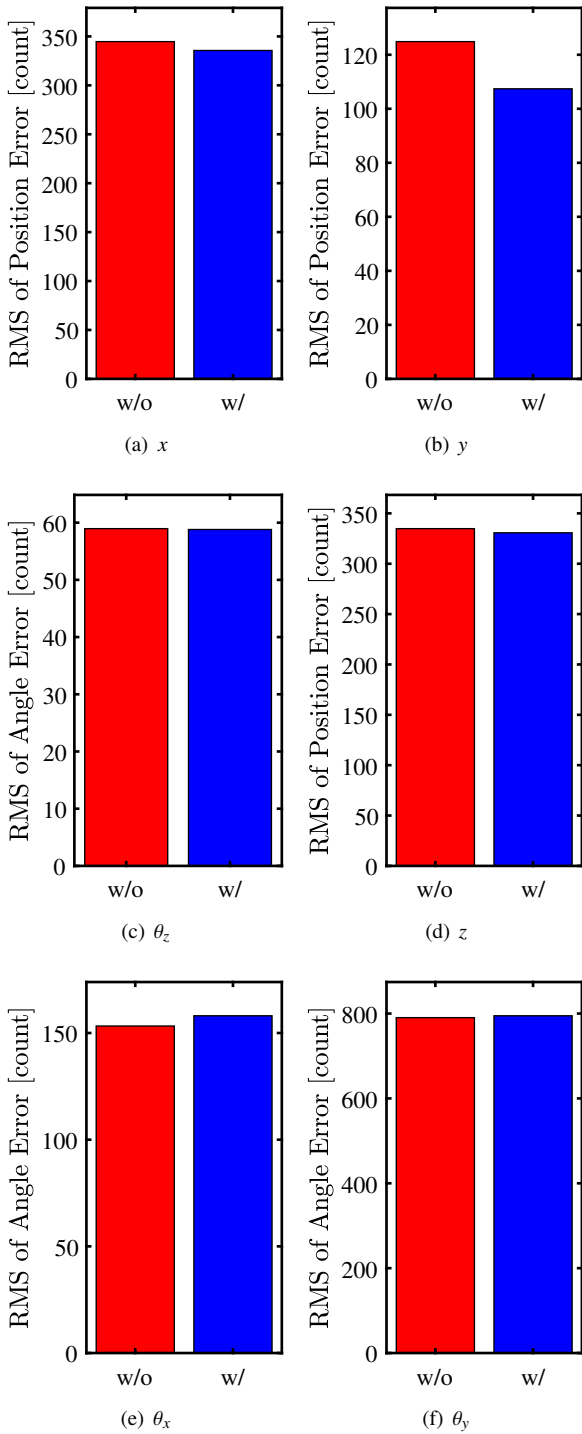
Figure 18: Root Mean Square (RMS) errors of a total of four scan regions in 6-DOFs ($x, y, \theta_z, z, \theta_x, \theta_y$). No peak filter is used in w/o (red bar ■) and one peak filter of translation along the x-axis with optimized condition is used in w/ (blue bar ■).

References

[1] T. Oomen, Advanced Motion Control for Precision Mechatronics: Control, Identification, and Learning of Complex Systems, IEEJ Journal of Industry Applications 7 (2) (2018) 127–140. doi:10.1541/ieejjia.7.127.
URL https://www.jstage.jst.go.jp/article/ieejjia/7/2/7_127/_article

[2] K. Sakata, H. Asaumi, K. Hirachi, K. Saiki, H. Fujimoto, Self Resonance Cancellation Techniques for a Two-Mass System and Its Application to a Large-Scale Stage, IEEJ Journal of Industry Applications 3 (6) (2014) 455–462. doi:10.1541/ieejjia.3.455.
URL http://jlc.jst.go.jp/DN/JST.JSTAGE/ieejjia/3.455?lang=en&from=CrossRef&type=abstract

[3] H. Fujimoto, Y. Hori, A. Kawamura, Perfect tracking control based on multirate feedforward control with generalized sampling periods, IEEE Transactions on Industrial Electronics 48 (3) (2001) 636–644. doi:10.1109/41.925591.
URL http://ieeexplore.ieee.org/document/925591/

[4] M. Mae, W. Ohnishi, H. Fujimoto, MIMO multirate feedforward controller design with selection of input multiplicities and intersample behavior analysis, Mechatronics 71 (February) (2020) 102442. doi:10.1016/j.mechatronics.2020.102442.
URL https://doi.org/10.1016/j.mechatronics.2020.102442

[5] H. Butler, Position Control in Lithographic Equipment [Applications of Control], IEEE Control Systems 31 (5) (2011) 28–47. doi:10.1109/MCS.2011.941882.
URL https://ieeexplore.ieee.org/document/6021296/

[6] W. Ohnishi, H. Fujimoto, K. Sakata, K. Suzuki, K. Saiki, Design and control of 6-DOF high-precision scan stage with gravity canceller, in: 2014 American Control Conference, IEEE, 2014, pp. 997–1002. doi:10.1109/ACC.2014.6859023.
URL http://ieeexplore.ieee.org/document/6859023/

[7] M. Mae, W. Ohnishi, H. Fujimoto, Y. Hori, Perfect Tracking Control Considering Generalized Controllability Indices and Application for High-Precision Stage in Translation and Pitching, IEEJ Journal of Industry Applications 8 (2) (2019) 263–270. doi:10.1541/ieejjia.8.263.
URL https://www.jstage.jst.go.jp/article/ieejjia/8/2/8_263/_article

[8] N. Dirkx, J. van de Wijdeven, T. Oomen, Frequency Response Function identification for multivariable motion control: Optimal experiment design with element-wise constraints, Mechatronics 71 (June) (2020) 102440. doi:10.1016/j.mechatronics.2020.102440.
URL https://doi.org/10.1016/j.mechatronics.2020.102440https://linkinghub.elsevier.com/retrieve/pii/S0957415820301100

[9] K. Tang, Kim Fung Man, Guanrong Chen, S. Kwong, An optimal fuzzy PID controller, IEEE Transactions on Industrial Electronics 48 (4) (2001) 757–765. doi:10.1109/41.937407.
URL http://ieeexplore.ieee.org/document/937407/

[10] S. Lee, N. Marsolan, T. Sun, S. Lee, B. Kilian, Application of Self-Optimizing Controllers to Variable Time-Delay Processes, in: Proceedings of the 1985 American Control Conference, 1985, pp. 1275–1280. doi:10.23919/ACC.1985.4788815.

[11] Z.-L. Gaing, A Particle Swarm Optimization Approach for Optimum Design of PID Controller in AVR System, IEEE Transactions on Energy Conversion 19 (2) (2004) 384–391. doi:10.1109/TEC.2003.821821.
URL http://ieeexplore.ieee.org/document/1300705/

[12] A. Karimi, G. Galdos, Fixed-order H infinity controller design for non-parametric models by convex optimization, Automatica 46 (8) (2010) 1388–1394. doi:10.1016/j.automatica.2010.05.019.
URL http://dx.doi.org/10.1016/j.automatica.2010.05.019

[13] T. M. T. Do, T. Artieres, Regularized bundle methods for convex and non-convex risks, Journal of Machine Learning Research 13 (2012) 3539–3583.

[14] R. Kitayoshi, H. Fujimoto, Automatic adjustment method of controller structure and parameter based on Structured H infinity control, in: IECON 2019 - 45th Annual Conference of the IEEE Industrial Electronics Society, 2019, pp. 3111–3116.

[15] M. Hast, K. Astrom, B. Bernhardsson, S. Boyd, PID design by convex-concave optimization, in: 2013 European Control Conference (ECC), IEEE, 2013, pp. 4460–4465. doi:10.23919/ECC.2013.6669312.
URL https://ieeexplore.ieee.org/document/6669312/

[16] S. Shinoda, K. Yubai, D. Yashiro, J. Hirai, Multivariable Controller Design Achieving Diagonal Dominance Using Frequency Response Data, Electronics and Communications in Japan 100 (10) (2017) 12–23. doi:10.1002/ecj.11970.
URL http://doi.wiley.com/10.1002/ecj.11970

[17] W. Ohnishi, Data-based feedback controller tuning utilizing collocated and non-collocated sensors, in: Joint 8th IFAC Symposium on Mechatronic Systems and 11th IFAC Symposium on Nonlinear Control Systems, 2019.

[18] M. Mae, W. Ohnishi, H. Fujimoto, K. Sakata, A. Hara, Peak Filter Tuning based on Disturbance Spectrum for MIMO High-Precision Scan Stage, in: IFAC World Congress 2020, 2020.

[19] A. L. Yuille, A. Rangarajan, The Concave-Convex Procedure, Neural Computation 15 (4) (2003) 915–936. doi:10.1162/08997660360581958.
URL http://www.mitpressjournals.org/doi/10.1162/08997660360581958

[20] H. Fujimoto, Y. Hori, Vibration suppression and optimal repetitive disturbance rejection control in semi-Nyquist frequency region using multirate sampling control, in: Proceedings of the 39th IEEE Conference on Decision and Control (Cat. No.00CH37187), Vol. 4, IEEE, 2000, pp. 3745–3750. doi:10.1109/CDC.2000.912292.
URL http://ieeexplore.ieee.org/document/912292/

[21] H. Fujimoto, T. Takemura, High-Precision Control of Ball-Screw-Driven Stage Based on Repetitive Control Using n-Times Learning Filter, IEEE Transactions on Industrial Electronics 61 (7) (2014) 3694–3703. doi:10.1109/TIE.2013.2290286.
URL https://ieeexplore.ieee.org/document/6661341/

[22] X. Chen, M. Tomizuka, New Repetitive Control With Improved Steady-State Performance and Accelerated Transient, IEEE Transactions on Control Systems Technology 22 (2) (2014) 664–675. doi:10.1109/TCST.2013.2253102.
URL http://ieeexplore.ieee.org/document/6508823/

[23] T. Atsumi, A. Okuyama, M. Kobayashi, Track-Following Control Using Resonant Filter in Hard Disk Drives, IEEE/ASME Transactions on Mechatronics 12 (4) (2007) 472–479. doi:10.1109/TMECH.2007.901944.
URL http://ieeexplore.ieee.org/document/4282597/http://ieeexplore.ieee.org/document/4291569/

[24] K. Sakata, FPD Exposure System and Precision Servo Technology (in Japanese), The Journal of the Institute of Electrical Engineers of Japan 137 (1) (2017) 19–22. doi:10.1541/ieejjournal.137.19.
URL https://www.jstage.jst.go.jp/article/ieejjournal/137/1/137_19/_article/-char/ja/

[25] J. Zheng, G. Guo, Y. Wang, W. Wong, Optimal Narrow-Band Disturbance Filter for PZT-Actuated Head Positioning Control on a Spinstand, IEEE Transactions on Magnetics 42 (11) (2006) 3745–3751. doi:10.1109/TMAG.2006.881290.
URL http://ieeexplore.ieee.org/document/1715685/

[26] Nikon, FPD Lithography Systems FX-103SH/103S (2019).
URL https://www.nikon.com/products/fpd/lineup/pdf/FX-103SH_103S_e.pdf

[27] B. A. Francis, W. M. Wonham, The internal model principle for linear multivariable regulators, Applied Mathematics & Optimization 2 (2) (1975) 170–194. doi:10.1007/BF01447855.
URL http://link.springer.com/10.1007/BF01447855

[28] T. Atsumi, W. C. Messner, Optimization of Head-Positioning Control in a Hard Disk Drive Using the RBode Plot, IEEE Transactions on Industrial Electronics 59 (1) (2012) 521–529. doi:10.1109/TIE.2011.2143377.
URL http://ieeexplore.ieee.org/document/5751673/

[29] Y. Maeda, M. Iwasaki, Circle Condition-Based Feedback Controller Design for Fast and Precise Positioning, IEEE Transactions on Industrial Electronics 61 (2) (2014) 1113–1122. doi:10.1109/TIE.2013.2257148.
URL http://ieeexplore.ieee.org/document/6494628/

[30] H. Rosenbrock, Design of multivariable control systems using the inverse Nyquist array, Proceedings of the Institution of Electrical Engineers 116 (11) (1969) 1929. doi:10.1049/piee.1969.0354.
URL DesignofmultivariablecontrolsystemsusingtheinverseNyquistarr

//digital-library.theiet.org/content/journals/10.1049/piee.1969.0354

[31] M. Araki, O. Nwokah, Bounds for closed-loop transfer functions of multivariable systems, IEEE Transactions on Automatic Control 20 (5) (1975) 666–670. `arXiv:arXiv:1011.1669v3`, `doi:10.1109/TAC.1975.1101051`.
URL http://ieeexplore.ieee.org/document/1101051/

[32] N. Sebe, Diagonal dominance and integrity, in: Proceedings of 35th IEEE Conference on Decision and Control, Vol. 2, IEEE, 1996, pp. 1904–1909. `doi:10.1109/CDC.1996.572854`.
URL http://ieeexplore.ieee.org/xpls/abs_all.jsp?arnumber=572854http://ieeexplore.ieee.org/document/572854/

[33] K. Nakamura, K. Yubai, D. Yashiro, S. Komada, Fully Parameterized Controller Design Method for High Control Bandwidth Using Frequency Response Data Sets, in: The 3rd IEEJ international workshop on Sensing, Actuation, Motion Control, and Optimization (SAMCON 2017), 2017.

[34] J. Lofberg, YALMIP : a toolbox for modeling and optimization in MAT-LAB, in: 2004 IEEE International Conference on Robotics and Automation (IEEE Cat. No.04CH37508), IEEE, 2004, pp. 284–289. `doi:10.1109/CACSD.2004.1393890`.
URL http://ieeexplore.ieee.org/document/1393890/

[35] MosekApS, MOSEK Optimization Toolbox for MATLAB 9.0.88 (2019).
URL https://www.mosek.com

[36] W. Ohnishi, H. Fujimoto, K. Sakata, K. Suzuki, K. Saiki, Decoupling Control Method for High-Precision Stages using Multiple Actuators considering the Misalignment among the Actuation Point, Center of Gravity, and Center of Rotation, IEEJ Journal of Industry Applications 5 (2) (2016) 141–147. `doi:10.1541/ieejjia.5.141`.
URL https://www.jstage.jst.go.jp/article/ieejjia/5/2/5_141/_article

[37] W. R. Abdul-Adheem, I. K. Ibraheem, Decoupled control scheme for output tracking of a general industrial nonlinear MIMO system using improved active disturbance rejection scheme, Alexandria Engineering Journal 58 (4) (2019) 1145–1156. `doi:10.1016/j.aej.2019.09.016`.
URL https://doi.org/10.1016/j.aej.2019.09.016https://linkinghub.elsevier.com/retrieve/pii/S1110016819301024